Supplement of Atmos. Meas. Tech., 15, 945–964, 2022
https://doi.org/10.5194/amt-15-945-2022-supplement
© Author(s) 2022. CC BY 4.0 License.

Atmospheric Measurement Techniques
Open Access
EGU

Supplement of

Detection of nitrous acid in the atmospheric simulation chamber SAPHIR using open-path incoherent broadband cavity-enhanced absorption spectroscopy and extractive long-path absorption photometry

Sophie Dixneuf et al.

Correspondence to: Albert A. Ruth (a.ruth@ucc.ie)

The copyright of individual parts of the supplement might differ from the article licence.

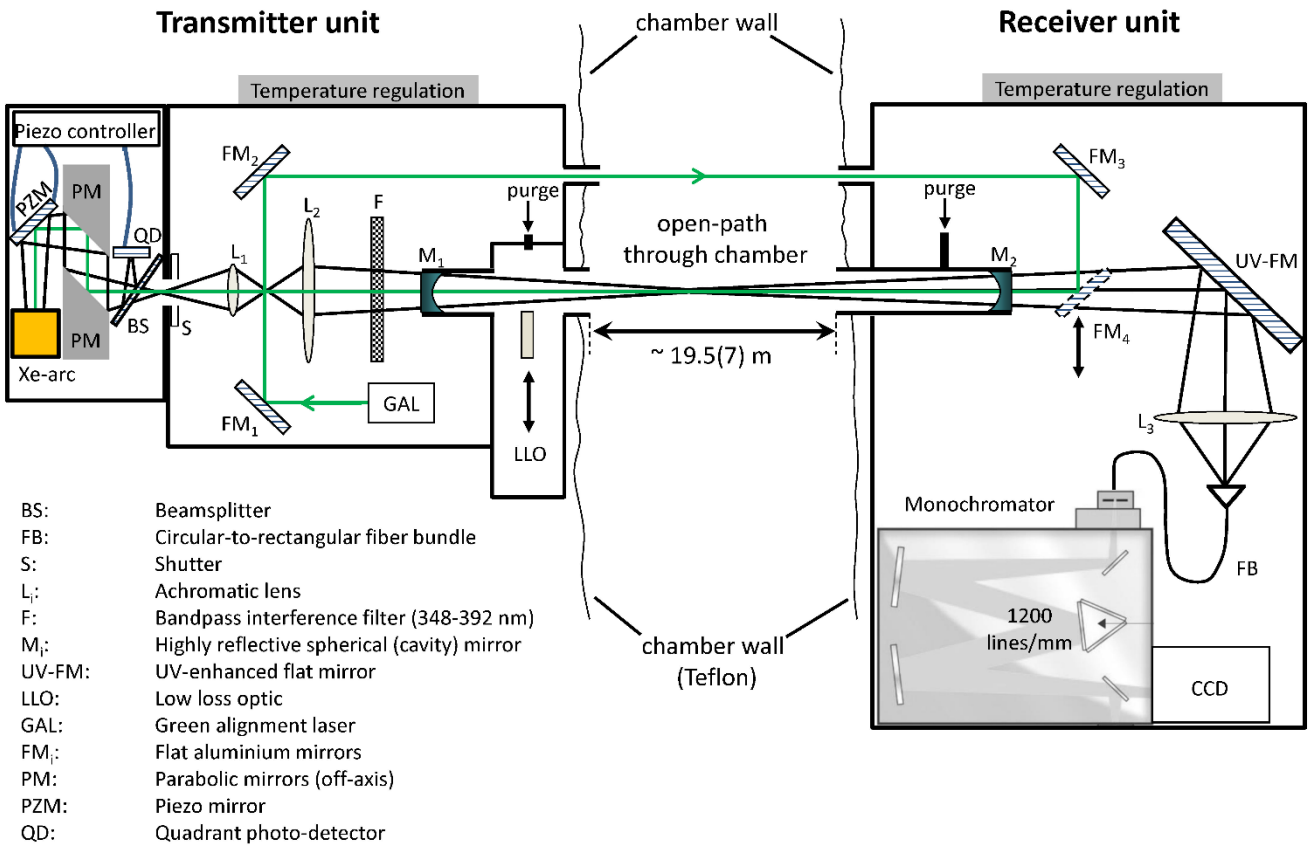

Figure S1: Schematic of the experimental IBBCEAS setup at the atmospheric simulation chamber SAPHIR at Jülich, Germany. The cavity mirrors (M_i) have a radius of curvature of r = –21 m and a diameter of 40 mm (Layertec GmbH). The mirror separation was l = 20.4 ± 0.1 m and the effective sample length inside the cavity was d = 19.5(7) m. The mirrors were purged with zero air at a flow rate of 1.7 SLPM. The light transmitted by the cavity was collected with an achromatic lens and coupled into a multimode quartz fibre bundle (FB, circular to rectangular), which was connected to a polychromator (Shamrock 303i, grating 1200 lines mm^{-1}, spectral resolution 0.21 nm) inside the receiver unit. The dispersed light was then detected by a cooled back-illuminated charged coupled device (CCD, Andor Newton).

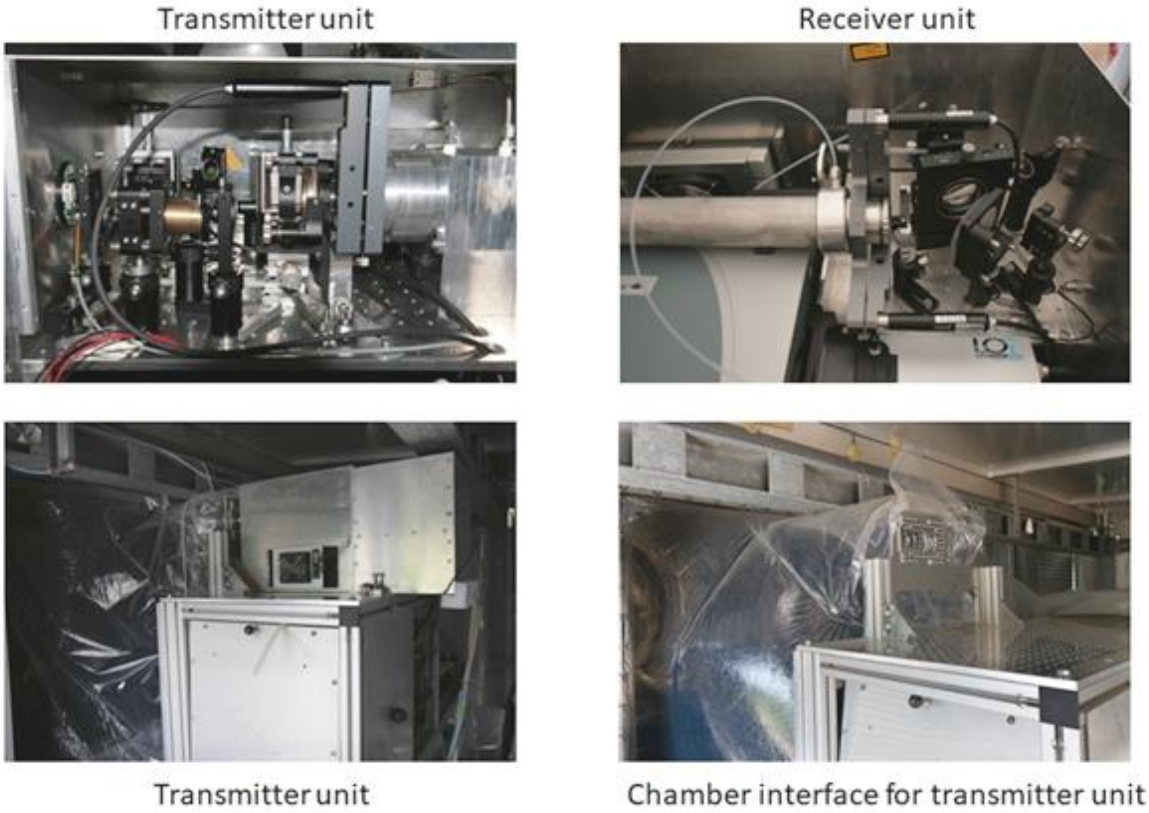

Figure S2: Photographs of the interior of the transmitter unit (upper left) and receiver unit (upper right), the mounting position of the transmitter unit on top of a frame bolted to a massive concrete support bench (lower left), and interface plate on the pressurized Teflon chamber foil before installation of the transmitter unit (lower right).

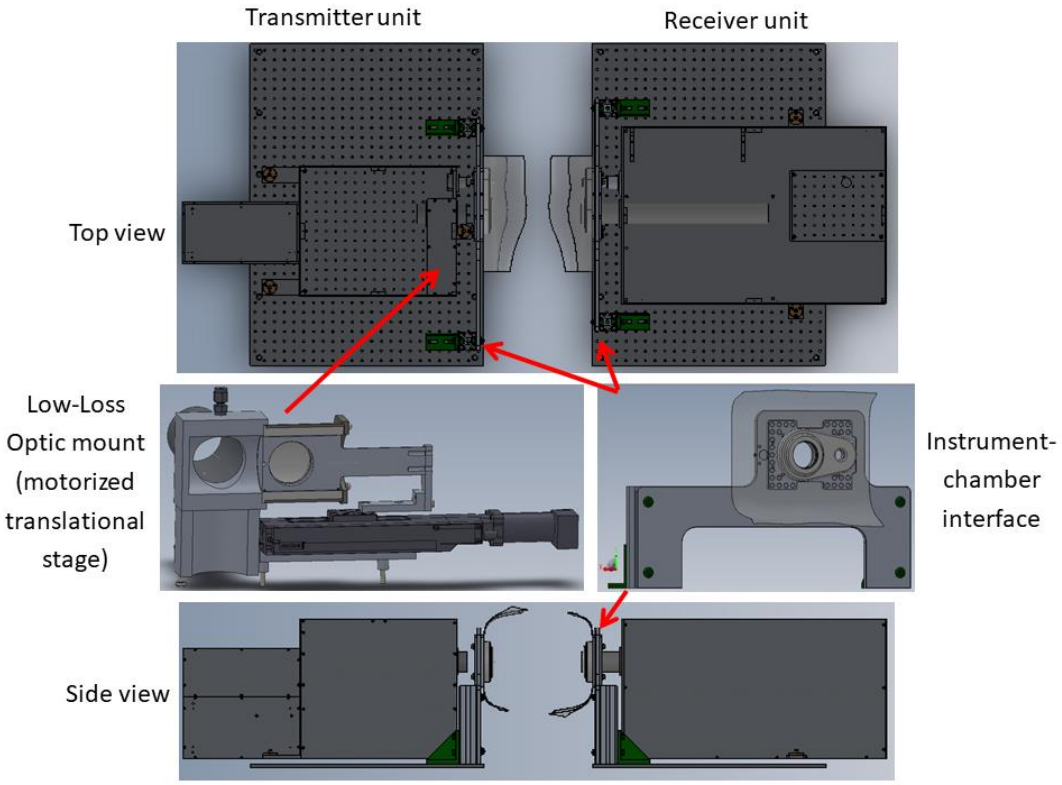

Figure S3: Upper Panel: Drawings of the top view of the transmitter and receiver units schematically. The low loss optic mount was installed inside the transmitter unit. Middle panel (left): Low loss optic mount on translational stage. While not in use the low loss optic was completely enclosed. The mount was also purged with zero air. Middle Panel (right): Drawing of the plates with feedthrough holes that were used to interface the units to the chamber (walls). Lower Panel: Drawings of the side view of the transmitter and receiver units schematically. The interface to the chamber is also shown on both sides.

ADDITIONAL INFORMATION ON LOW-LOSS OPTIC (LLO)

The role and use of the low loss optic and its features can also be found in Ruth et al. 2014, Varma et al. 2009, Ruth and Lynch 2008:

$$R_{\mathrm{eff}}(\lambda) = 1 - \left(\frac{I(\lambda)}{I_0(\lambda) - I(\lambda)}\, d\varepsilon(\lambda) \right) \qquad (\mathrm{S.eq.}\,1)$$

If the mixing ratio of, e.g. NO_2 is known from a CLS measurement (in an otherwise clean chamber), then ε is known from the known cross-section spectrum of NO_2. By measuring I_0 and I and knowing the effective cavity length d, the reflectivity spectrum can be calculated (Ruth et al. 2014). Once the reflectivity, R_{eff}, is known from an NO_2 calibration measurement, the optical loss of the low loss (anti-reflection coated) optic (LLO) can also be measured accurately. This is typically done at the time of the initial calibration of R_{eff} (see Figure S4). The low loss optic can then be used to determine the reflectivity, using the latest "up-to-date" I_0 measurement, typically taken in the morning after extensive overnight flushing, when the chamber is clean. However, during an experiment with sample mixture in the chamber, the LLO is merely used to check for changes in the reflectivity. In the clean chamber in principle the LLO essentially takes the place of the NO_2 calibration gas. In the filled chamber, however, insertion of the LLO cannot be used to independently measure absolute reflectivities anymore but only relative changes of same. With target species (and additional loss) in the chamber, one can only retrieve the absolute reflectivity, if I_0 has not changed since its last measurement (in the morning for example). Hence one cannot distinguish between a change of R_{eff} and a change of I_0 based on the LLO measurement (compare eq. (2) in the main text). One can however figure out how far the setup has drifted from the initial measurement (typically in the morning).

This is a general problem of open path measurements where I_0 cannot easily be established at regular intervals. In closed path setups (extractive instruments) an accurately calibrated LLO can be used for reflectivity calibration because a new I_0 spectrum can be created readily every time the reflectivity is to be checked based on eq. (2).

It is recommended to check from time to time how accurate the calibration of the LLO still is. Typical calibration measurements are shown in the supplementary material using NO_2 (Figure S5) and the LLO (Figure S4).

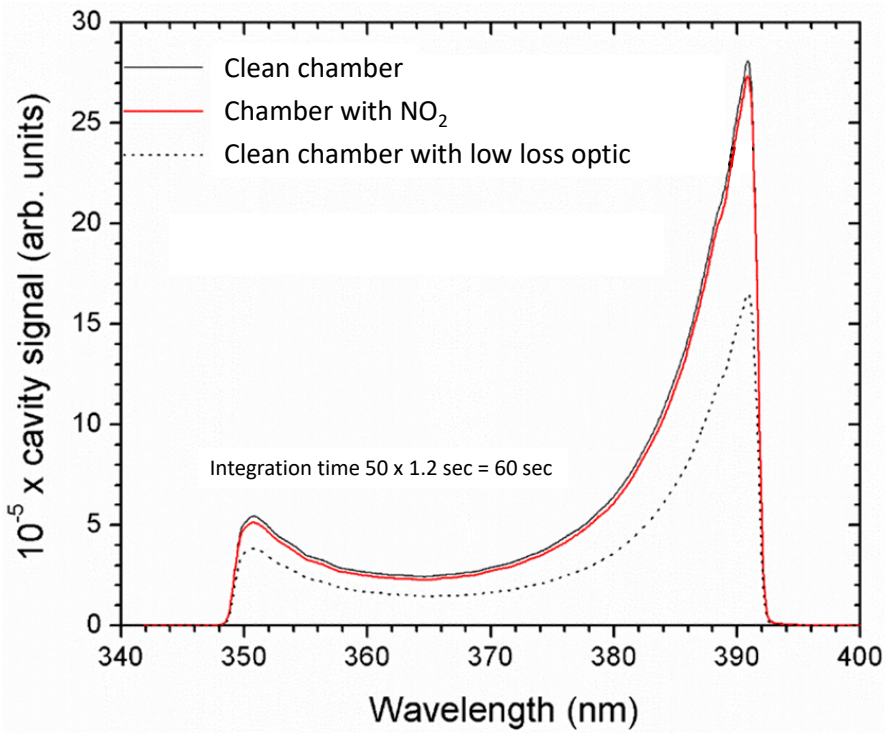

Figure S4: Examples of transmission spectra of the long cavity for a total integration time of 1 min. The signal below ~350 nm and above ~390 nm was suppressed by a single bandwidth filter (Semrock FF01-370/36) with cut-on and cut-off wavelength of 348 nm and 392 nm respectively. Gray trace: $I_0(\lambda)$, intensity transmitted by the cavity for a chamber that was flushed overnight with zero air (clean chamber). Red line: $I(\lambda)$, intensity transmitted by the cavity for a chamber that was primed with NO_2 in a reflectivity calibration measurement. Dashed line: Same as gray trace, but with the low loss optic in the beam.

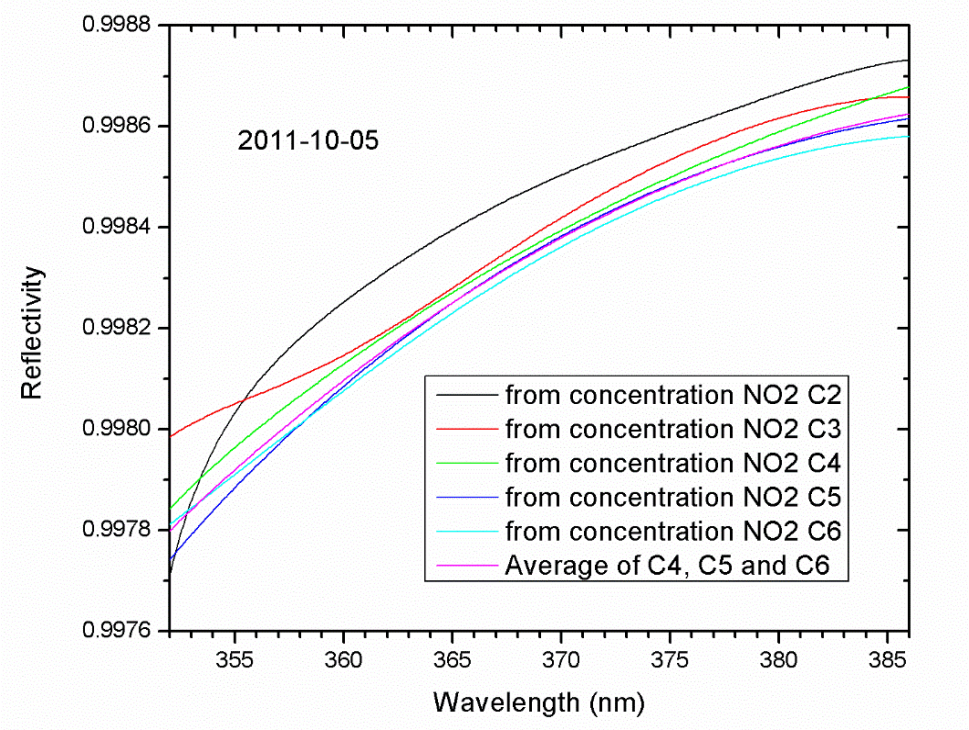

Figure S5: Reflectivity spectra, $R(\lambda)$, for 5 different concentrations (C2…C6) of NO_2 during the measurement on 5 October 2011. The trace in magenta shows the average of three measurements with different concentrations, which was used to establish the reflectivity spectrum of the mirrors.

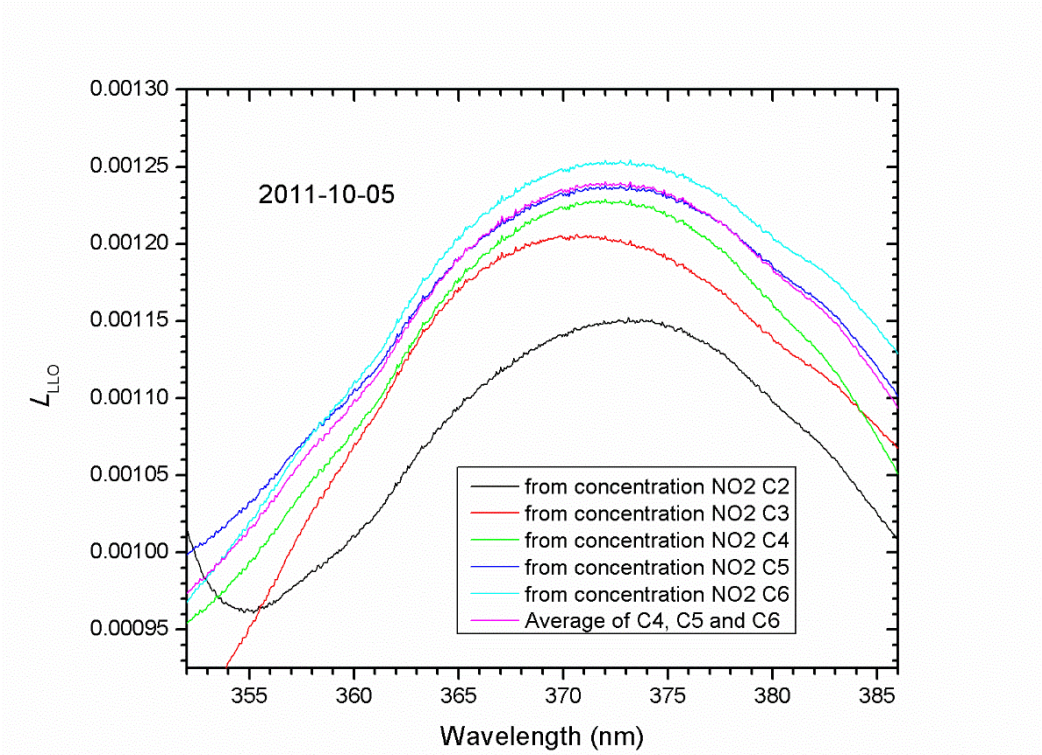

Figure S6: Example of a loss spectrum, $L_{LLO}(\lambda)$, of an antireflection coated optic ("low loss optic", LLO), used to determine the reflectivity in the morning after flushing the chamber (see Figure S4). The loss was calibrated from measurements with NO_2 at different concentrations (see Figure S5). The trace in magenta shows the average of three measurements with different concentrations, which was used to establish the loss spectrum of the LLO.

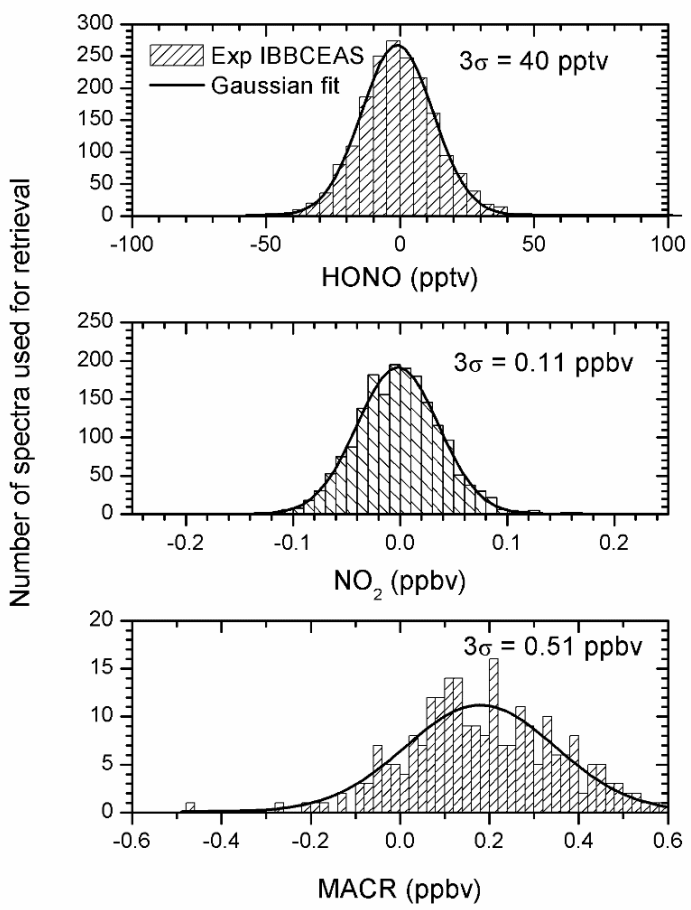

Figure S7: Establishment of the 3σ limit of detection (LOD) of the IBBCEAS instrument for a 1 min acquisition time. From the 1σ standard deviation of the residuals of individual spectral fits the distribution of deviations was established from which the LOD was determined to be ~39 pptv for HONO, ~114 pptv for NO_2, and ca. 510 pptv for MACR in the 352-386 nm wavelength range used for the fit.

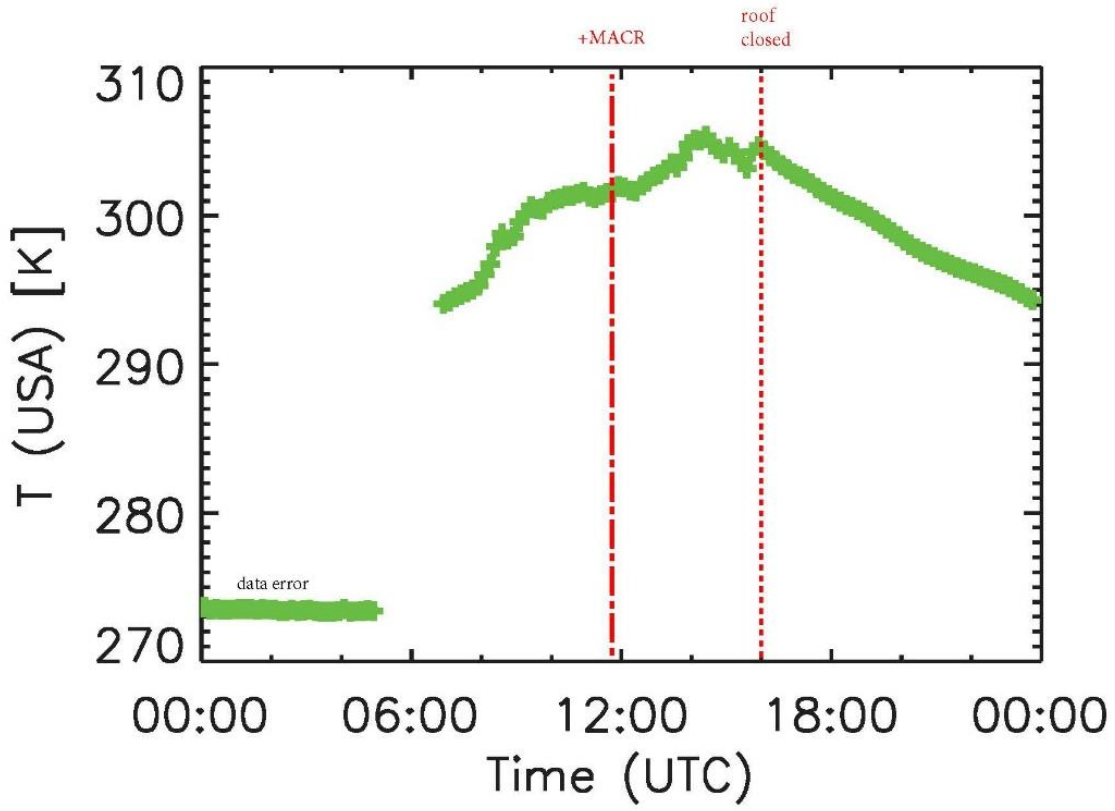

Figure S8: Temperature in the chamber as a function of time measured on 11 July 2011. The temperature was measured with an ultrasonic anemometer (USA). Between the addition of MACR (vertical dashed-dotted line) and the closing of the roof (vertical dotted line), the temperature was > 300K.

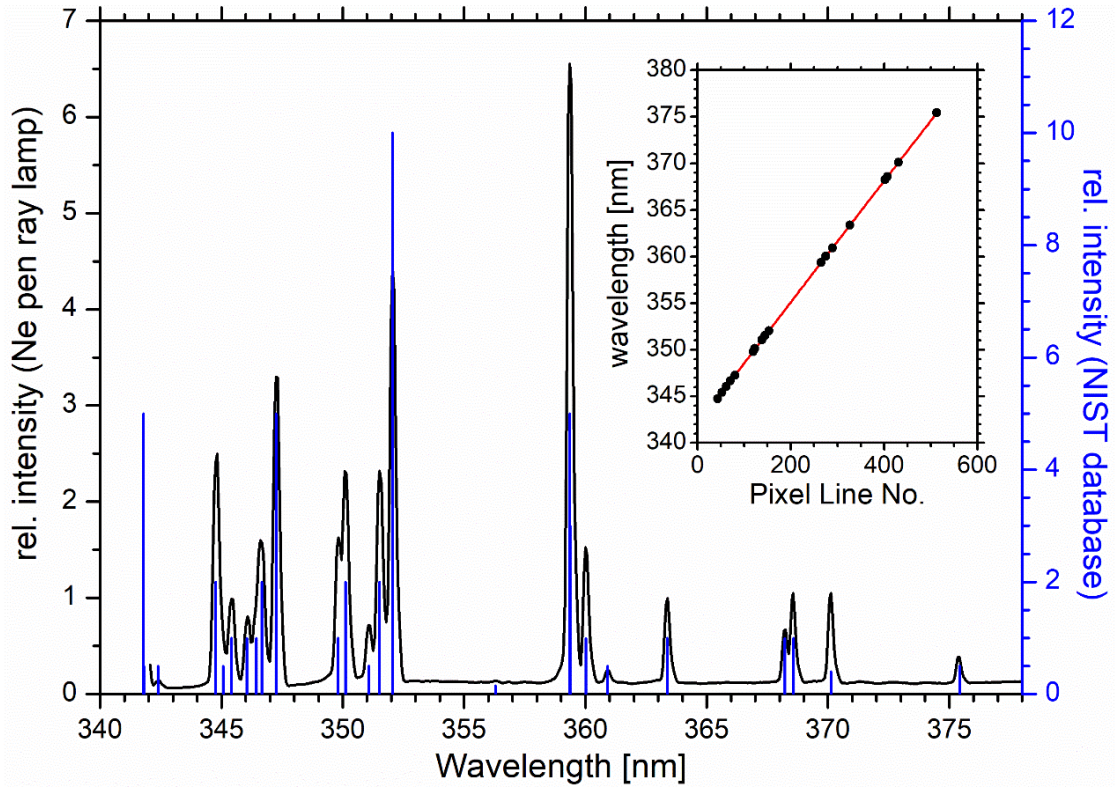

Figure S9: Black trace - measured spectrum from a Ne pen ray lamp. Blue trace – line position and relative intensity from the NIST database (https://physics.nist.gov/PhysRefData/Handbook/Tables/neontable7.htm); (Saloman and Sansonetti 2004).

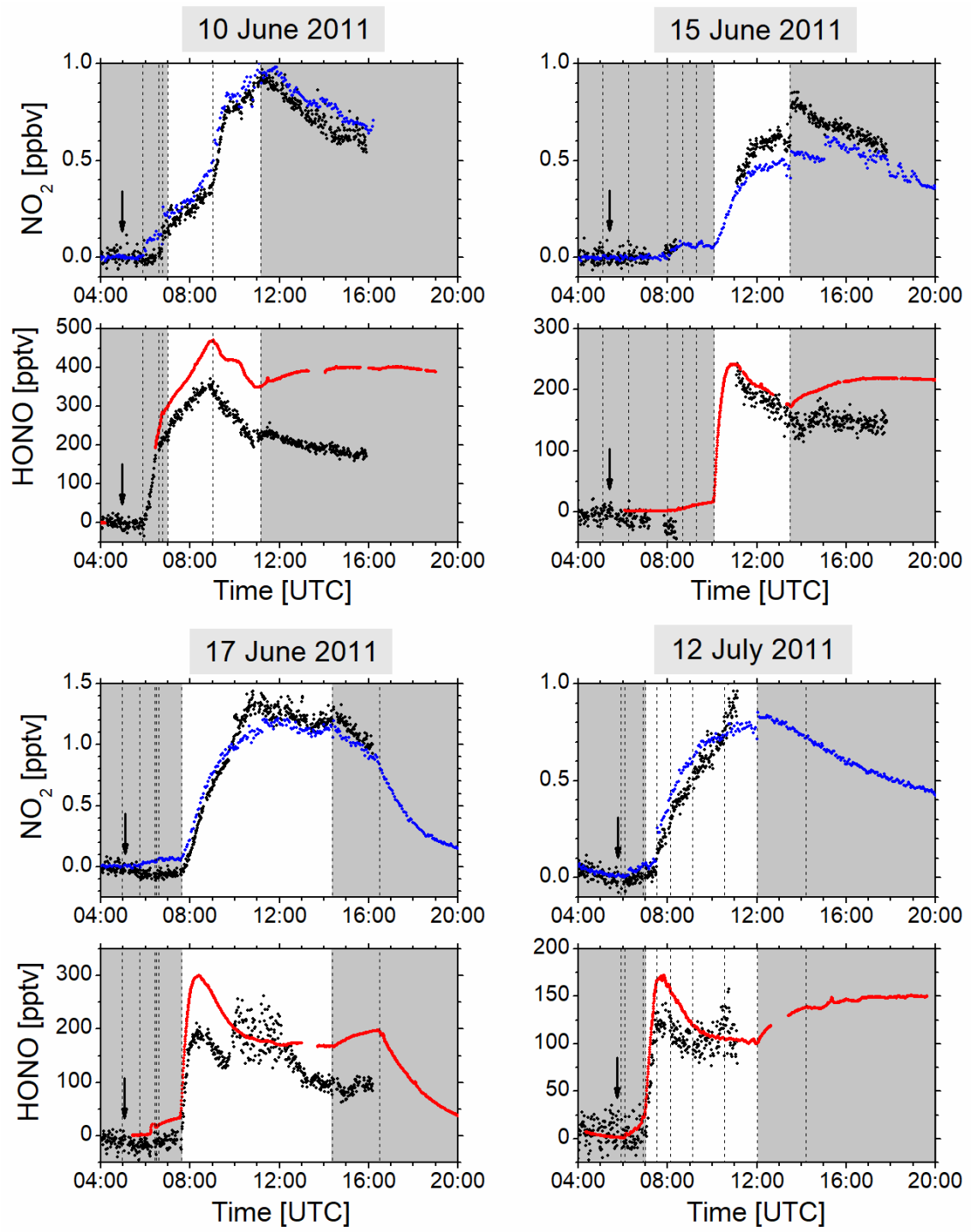

Figure S10:
<u>10 June 2011</u>: Start of humidification (5:55), end of humidification (6:35), O_3 addition (6:45), roof opened (7:00), isoprene addition (9:00), roof closed (11:12) – upper left two panels.
<u>15 June 2011</u>: Flushing of chamber stopped (5:05), isoprene addition (6:15), start of humidification (8:00), end of humidification (8:38), O_3 addition (9:15), roof opened (10:05), roof closed (13:30) – upper right two panels.
<u>17 June 2011</u>: Flushing of chamber stopped (04:58), start of humidification (05:45), end of humidification (06:25), O_3 addition (06:30), CO addition (06:35), roof opened (07:36), roof closed (14:23), flushing of chamber started (16:29) – lower left two panels.
<u>12 July 2011</u>: Flushing of chamber stopped (05:55), start of humidification (06:05), end of humidification (06:55), roof opened (07:00), 40 ppb O_3 (07:30), isoprene (08:08), isoprene (09:08), isoprene (10:33), roof closing (12:00), ventilator off (14:13) – lower right two panels.
The vertical black arrows indicate the times when measurements of I_0 in the "clean chamber" were taken. Grey area = dark conditions, white area = light-filled chamber; IBBCEAS data (black), LOPAP (red), CLS (blue).

OPEN PATH IBBCEAS INSTRUMENT IN COMPARISON WITH OTHER INSTRUMENTS

A comparison of IBBCEAS instruments from the recent literature can be found in Table 1 of the article by Jordan and Osthoff 2020. A link to this particular Table is provided here:
amt.copernicus.org/articles/13/273/2020/amt-13-273-2020-t01.png
See also Table 1 in Tang et al. 2020. The relevant experimental parameters of the current open path IBBCEAS instrument are listed here for comparison:

Light source manufacturer:	Analytic Jena
Model:	n/a
Power [W]:	<0.44*
Center (peak) wavelength and spectral width [nm]:	370 ± 20
Fit range [nm]:	352 – 386
Mirror reflectivity:	0.9978 – 0.9986
Cavity (sample) length [m]:	19.57
Effective pathlength [km]:	~9.8
Acquisition time [s]:	60
HONO 2σ LOD [ppbv]:	0.076

*18 W cm^{-2} sr^{-1} nm^{-1} at 400 nm. For a hot spot size of 150 μm this translates into an estimated maximally collectable optical power of roughly ~440 mW in the relevant spectral range based on the optics in the transmitter unit. This is an upper limit of the optical power that is incident on the first cavity mirror; the true value can be estimated to be significantly smaller by up to ~40% due to reflection and diffraction losses in the imaging process.

REFERENCES

Jordan, N., and Osthoff, H. D.: Quantification of nitrous acid (HONO) and nitrogen dioxide (NO_2) in ambient air by broadband cavity-enhanced absorption spectroscopy (IBBCEAS) between 361–388 nm, Atmos. Meas. Tech., 13, 273-285, doi: 10.5194/amt-13-273-2020, 2020.

Saloman, E. B., and Sansonetti, C. J.: Wavelengths, energy level classifications, and energy levels for the spectrum of neutral neon, J. Phys. Chem. Ref. Data, 33, 1113-1158, doi: 10.1063/1.1797771, 2004.

Tang, K., Qin, M., Fang, W., Duan, J., Meng, F., Ye, K., Zhang, H., Xie, P., He, Y., Xu, W., Liu, J., and Liu, W.: Simultaneous detection of atmospheric HONO and NO2 utilising an IBBCEAS system based on an iterative algorithm, Atmos. Meas. Tech., 13, 6487–6499, doi: 10.5194/amt-13-6487-2020, 2020.